Scale decomposition of unstable growing fronts

Z. Moktadir*
School of Electronics and Computer Science, Southampton University, Southampton, United Kingdom
(Received 6 October 2003; revised manuscript received 27 February 2004; published 7 July 2004)

We present results obtained from the wavelet transform of unstable growing fronts. The linear growth equation is transformed using the Hermitian wavelets obtained from recursive shifts and changes in the Gaussian filters. We explore the evolution of the instability at different scales, and at different locations (in the direct space) in the wavelet domain, using a numerical growth model and the experimental example of chemically etched silicon. Wavelet formalism may have an advantage over Fourier methods in the sense that one can track the instability in the location (direct space) and at different scales simultaneously. It also provides a quantitative tool for the characterization of the growing fronts through its concise scale discrimination.

DOI: 10.1103/PhysRevE.70.011602 PACS number(s): 81.15.Aa, 02.70.−c, 05.40.−a, 05.70.Ln

I. INTRODUCTION

A variety of growth and erosion phenomena can be described by stochastic partial differential equations. Epitaxial growth is an example in which atoms are deposited on the substrate, where they become attached to other atoms or undergo diffusion. In homoepitaxial growth, deposited atoms and substrate, atoms are the same. Consequently, there is no lattice mismatch and the growth process is expected to be smooth. In fact, over a certain range of temperature, the growth process is a layer-by-layer process. A layer is entirely grown before the next layer starts to grow [1]. This is an ideal situation where one would like to achieve such smooth surfaces for technological applications. However, most of the time the resulting surfaces are rough, and the layer-by-layer process does not occur in such situations. In the epitaxial growth process mentioned above, the roughening of surfaces is explained by two processes: (i) The flux of deposited atoms is not constant, but fluctuates around a mean value. This induces a random noise in the growing process, and self-affine surfaces are obtained, exhibiting scaling properties in space and time [2,3]. (ii) An asymmetric diffusion barrier, called the Ehrlich-Schwoebel (ES) barrier, exists at the edges of atomic steps impeding a downhill flow of atoms across the step [4]. This asymmetry in attachment kinetics creates an instability for low temperature growth on vicinal surfaces, and this class of growth instability has since been observed in many experiments (see, for example, Ref. [5]).

The erosion of surfaces by ion sputtering gives rise to ripples on bombarded surfaces [6]. The ripple formation is attributed to an instability that is inherent in the erosion process itself, and it is linked to the surface curvature (see also Ref. [7]). For interested readers, excellent reviews of instabilities in growth of crystals and ion sputtering of surfaces can be found in Refs. [8–10].

On the other hand, etching of crystals is a very important part of today's micro technology. In microsystems, for example, chemical etching of silicon is a widely used technique in the fabrication of miniaturized structures [11,12]. In most cases, the resulting etched surfaces are rough in texture except for a few crystallographic orientations [12]. Very few attempts have been made to explain the roughening of surfaces during wet etching of silicon. It has been suggested in Ref. [13] that an instability resulting from the surface tension exists during the etching of Si(110).

In epitaxial growth, and in the presence of the ES barrier, the growing surface consists of regular mound structures. When diffusion is taken into account in the growth mechanism, the continuum equation describing the growth process was proposed by Johnson *et al.* [14]:

$$\frac{\partial h}{\partial t} = -\nu \nabla \frac{\nabla h}{1 + \nabla h^2} - K\nabla^4 h + \eta(x,t). \tag{1}$$

The term $\eta(x,t)$ is Gaussian white noise, such that $\langle \eta(x,t)\eta(x',t')\rangle = 2D\delta(x-x')\delta(t-t')$. This noise term reflects the stochastic character of the growth process. The first term on the right-hand side of Eq. (1) represents the up-hill growth due to the ES barrier effect, and the second term is due to the surface diffusion (capillary effect). This term has a stabilizing effect against the instability induced by ES barrier. The parameter $\nu > 0$ gives the attachment/detachment barrier at the surface edges, and $K > 0$ is proportional to the surface diffusion constant. At the early stage of growth, the slope ∇h is small and Eq. (1) becomes

$$\frac{\partial h}{\partial t} = -\nu\nabla^2 h - K\nabla^4 h + \eta(x,t). \tag{2}$$

Because the noise term is a random Gaussian process, $h(x,t)$ is also a random Gaussian process. Equation (2) can also describe the erosion of surfaces by ion bombardment [6]. However, the parameter ν arises from a different mechanism generated by the erosion process and it is given by $\nu = Fa\Omega Y_0 \Gamma$, where F is flux, a is ion energy penetration depth, Ω is atomic volume, Y_0 is sputtering yield, and Γ is a coefficient governing the erosion rate dependence on the local surface curvature.

A linear stability analysis reveals the instability of Eq. (2). Generally, this analysis is performed in Fourier space. Fourier analysis shows that in the linear regime small initial perturbations will grow in time to form the dominant feature of the surface texture (the dominant wavelength). A small perturbation (small q perturbation) will grow at a rate $\omega(q)$

*Electronic address: zm@ecs.soton.ac.uk

$=\nu q^2 - Kq^4$, resulting in a cellular local structure, corresponding to a critical wave number $q_c = \sqrt{\nu/K}$ and to a maximally unstable wave vector $q_{\max} = \sqrt{\nu/2K}$, corresponding to a dominant wavelength $\lambda_d = 2\pi\sqrt{2K/\nu}$.

We propose in this paper to analyze Eq. (2) in wavelet space. This will allow us to track of the growth instability in both direct and frequency (or scale) space at the same time, as opposed to Fourier analysis, in which the instability is studied only in the frequency space.

It is well known that a function can be expanded into a base function to represent it in a form adapted to a particular question. In harmonic analysis, for example, the signals obtained are sinusoids, and thus the suitable method of expansion is Fourier transformation. The generated height profiles from Eq. (2) have no sinusoidal shapes, but rather triangular shapes having a largely linear rise to the maximum and a subsequent linear decay. Another type of transformation using a suitable base functions should yield a more satisfying description. These base functions must have a shape intrinsically similar to that of the quick variations of the signal, permitting a resolution in frequency and space. An ideal candidate is the wavelet transform (WT), based on an appropriately chosen mother wavelet. The difference between the WTs and the Fourier transforms is that wavelet functions are localized in space, whereas the sine and cosine are not. A detailed description of the wavelet transform formalism is beyond the scope of this paper. See, for example, Ref. [15] for more information about the theory of wavelets. Wavelet analysis is capable of revealing aspects of data that other signal analysis techniques miss: aspects like trends, breakdown points, discontinuities in higher derivatives, and self-similarity. From an intuitive point of view, wavelet decomposition measures the degree of "resemblance" between the wavelet and the original signal. It is therefore suitable for detecting self-similarity or fractality of the signal. This degree of "resemblance" is represented by wavelet coefficients. If the signal (surface profile) is self-similar, then wavelet coefficients will be similar at different scales. This paper is organized as follows: Sec. II describes the Hermitian wavelets used in this work, and their properties. We also derive an evolution equation of the growth process in wavelet space in this section. In Sec. III we present results on the numerical computation of wavelet coefficients for the linear growth equation (2). In Sec. IV, a practical example of chemically etched silicon is discussed, and finally in Sec. V, our conclusion is presented.

II. WAVELET TRANSFORM OF UNSTABLE GROWING FRONTS

A. Hermitian wavelets and their properties

Wavelet analysis is the breaking up of a signal into shifted and scaled versions of the original (or mother) wavelet. That is,

$$\psi(a,b) = \frac{1}{\sqrt{a}}\psi\left(\frac{x-b}{a}\right), \tag{3}$$

where a ($a>0$) and b are, respectively, the scale parameter and the dilatation parameter, x is the space variable, and ψ is the mother wavelet. These basis functions vary in scale by slicing the data space using different scale sizes. The continuous wavelet transform (CWT) is defined as the sum over all of the surface profile multiplied by the shifted and scaled mother wavelet:

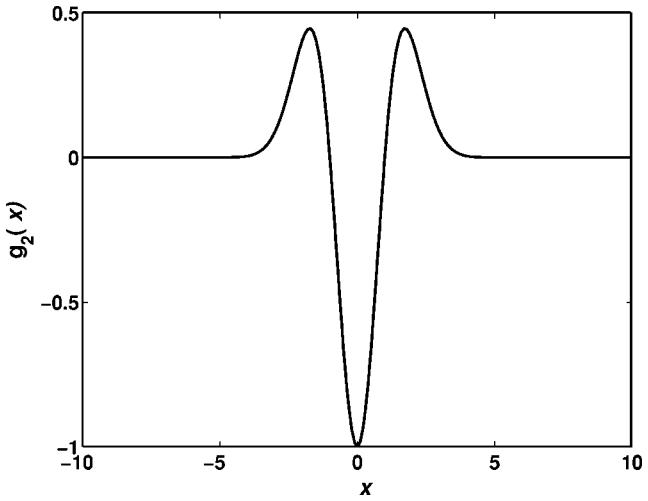

FIG. 1. A graphic representation of the Hermitian wavelet $g_2(x)$.

$$W(a,b) = \int h(x)\psi(a,b)dx. \tag{4}$$

$W(a,b)$ is the wavelet coefficient which is a function of the scale and the position. Then, CWT describes the surface profile in a given position b and a given scale a.

Hermitian wavelets [16] are particularly attractive because of their recursive property that allows one to transform linear partial differential equations from the direct space to wavelet space, as we will show in what follows. They are derived recursively from the Gaussian function $g_0(x) = e^{(-x^2/2)}$, i.e,

$$g_n(x) = -\frac{dg_{n-1}(x)}{dx} = (-1)^n P_n(x) g_0(x). \tag{5}$$

The function $g_0(x) = e^{(-x^2/2)}$ itself is not a wavelet. $P_n(x)$ is the Hermite polynomial of order n. The wavelets g_n satisfy the admissibility condition: $\int_{-\infty}^{\infty} g_n(x)dx = 0$. It is then possible to invert the wavelet transform. The well-known "Mexican Hat" wavelet is $-g_2(x) = (1-x^2)e^{(-x^2/2)}$, and is displayed in Fig. 1.

The wavelet transform of a height field $h(y,t)$ is defined as

$$u_n(\kappa,x,t) = \kappa^{1/2}\int_{-\infty}^{\infty} h(y,t) g_n[\kappa(y-x)]dy, \tag{6}$$

where we have adopted the notation from Ref. [17]. The variable κ is the inverse of the scale usually used in wavelet notation and is called the "wavelet number." Now let us put $\xi = \kappa(y-x)$. It is easy to show that the wavelets g_n satisfy the recursion relation

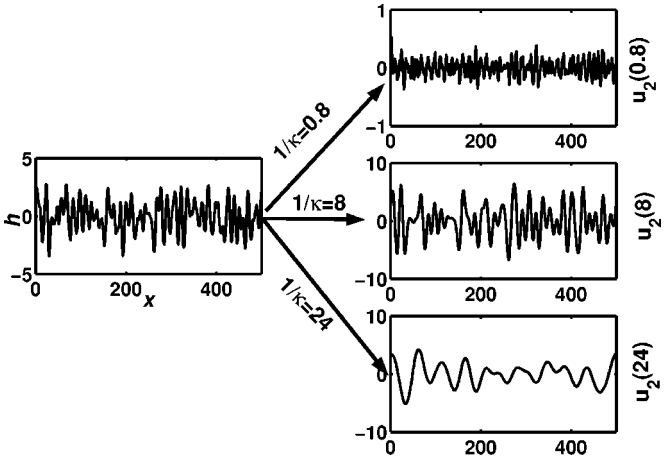

FIG. 2. The scale decomposition of the surface profile for $t=1.6$ and for three different scales: $1/\kappa=0.8$, 8, and 24. The wavelet $g_2(x)$ was used.

$$\frac{\partial^2}{\partial x^2}g_n(\xi) = -\kappa^3\frac{\partial}{\partial x}g_n(\xi) - (n+1)\kappa^2 g_n(\xi). \tag{7}$$

Using Eq. (7) combined with the definition (6) leads to the important relation

$$\frac{\partial}{\partial \kappa}u_n = -\frac{1}{\kappa^3}\frac{\partial^2}{\partial x^2}u_n - \frac{(n+1/2)}{\kappa}u_n. \tag{8}$$

This is true for any field h. We can also show the recursion relation:

$$\frac{\partial^i}{\partial x^i}u_n = \kappa^i u_{n+1}, \quad i=1,2,3,\ldots \tag{9}$$

One can define the wavelet power spectrum, or the *scalegram*, which is useful at picking out frequencies and calculating energy distributions:

$$W_n(\kappa,t) = \int_{-\infty}^{\infty}[|u_n(\kappa,x,t)|]^2 dx. \tag{10}$$

Relation (10) is the analog of the power spectrum used in Fourier analysis. This is a representation of the power contained in each scale $1/\kappa$. For a finite signal which is the case in a practical situation, this definition becomes $W_n(\kappa,x,t)=\langle|(u_n(\kappa,x,t)|^2\rangle_x$, where the brackets denote the spacial average over the variable x. Using this relation, one gets a location-invariant measure of power in a given scale.

In the next section, we will use the relations above to transform the stochastic partial differential equation (2) into the wavelet domain. This will lead to the evolution equation of wavelet coefficients defined by Eq. (6).

B. The growth equation in wavelet space

In the following, we will use the relations obtained in the last section to transform Eq. (2) into an evolution equation operating in the wavelet domain. However, our objective is not to solve this equation in the present work, but it is useful to derive it. Using the definition (6) we have

$$\frac{\partial}{\partial t}u_n = \sqrt{\kappa}\int_{-\infty}^{\infty}\nu\left(\frac{\partial^2}{\partial y^2}h\right)u_n(\kappa\,(y-x))dy - \sqrt{\kappa}\int_{-\infty}^{\infty}K\left(\frac{\partial^4}{\partial y^4}h\right)u_n(\kappa\,(y-x))dy + S(\kappa,x,t), \tag{11}$$

where

$$S_n(\kappa,x,t) = \sqrt{\kappa}\int_{-\infty}^{\infty}\eta(y,t)g_n(\kappa\,(y-x))dy \tag{12}$$

is the wavelet transform of the noise $\eta(y,t)$. Now, integrating both terms by parts on the right-hand side of Eq. (11), using Eqs. (9) and (10), and little bit of algebra, we finally arrive at

$$\frac{\partial}{\partial t}u_n = -H_1(\kappa)\frac{\partial^2}{\partial \kappa^2}u_n - H_2(\kappa)\frac{\partial}{\partial \kappa}u_n - H_3(\kappa)u_n + S(\kappa,x,t), \tag{13}$$

where

$$H_1(\kappa) = K\kappa^6,$$

$$H_2(\kappa) = K\kappa^6 + \nu(2n+1)\kappa^3,$$

$$H_3(\kappa) = K\kappa^4(n+1/2)^2 + \nu(n+1/2)\kappa^2. \tag{14}$$

Equation (13) is a stochastic partial differential equation operating in Hermitian wavelet space. This equation deserves, of course, more development, but it is beyond the scope of this paper. Instead, we will solve Eq. (2) in the physical space and transform the result into Hermitian wavelet space using the transform (6). We chose the latter because it was straightforward.

III. NUMERICAL DERIVATION OF THE WAVELET COEFFICIENTS FOR THE LINEAR GROWTH EQUATION

Equation (2) is discretized and solved numerically in one-dimensional space. Periodic boundary conditions are used. If the height h of the evolving front takes discrete values $\{h=h_i, i=1\ldots N\}$, where N is the system size, we have the iteration:

$$h_i(t+\Delta t) = h_i(t) + \Delta t(-\nu\nabla_i^2 h_i - K\nabla_i^4 h_i) + \Delta t\sqrt{\frac{12D}{\Delta t(\Delta x)^2}}r, \tag{15}$$

where r is a uniform random number between -1 and 1. ∇_i, ∇_i^2, and ∇_i^4 are the first-, second-, and fourth-order discretization operators, respectively.

Wavelets have the ability to split a surface profile up into components that are not pure sine waves, as opposed to Fourier transform. When summing all those components, one retrieves the exact profile. In Fig. 2 we show a splitted surface profile generated from Eq. (15), and transformed using the transform (6) and $g_2(x)$, for three different scales $1/\kappa=0.8$, 8, and 24 and for $t=1.6$. Note that high oscillations

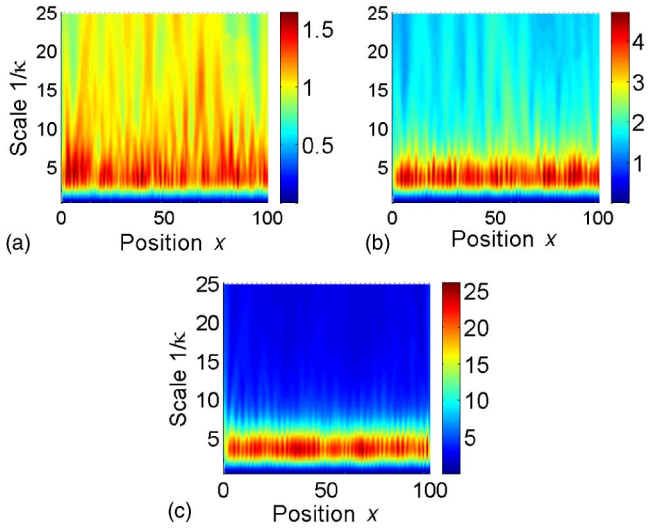

FIG. 3. (Color online) The magnitude of the wavelet coefficients of the height for three different times: (a) $t=0.6$, (b) $t=1.5$, and (c) $t=3$. The integration parameters are $\nu=1$, $D=0.05$, and $K=0.2$. The wavelet coefficients are obtained using the wavelet $g_2(x)$.

correspond to small scales, while low ones correspond to large scales, and also that the decomposition does not result in sine waves.

To follow the evolution of the growth instability in both scale and location, we perform the wavelet transform of the surface height for three different times: $t=0.6$, 1.5, and 3. Figure 3 shows the result for the magnitude of the wavelet transform. The system size is $L=250$ and the integration parameters are $\nu=1$, $D=0.05$, and $K=0.2$. The wavelet coefficients are obtained using the wavelet $g_2(x)$, and are averaged over 50 realizations. We notice that the magnitude of the wavelet transform u_n increases with time as one would expect from an unstable front. A band of scales corresponding to the maximum amplitude is clearly developing as time advances. The dominant scale (corresponding to the highest amplitude) lies in the middle of this band. At the early stage, the noise $\eta(y,t)$ initializes the growth at different scales. As time advances, large scales will grow, while small scales will decay, as clearly seen in Fig. 3 [either sides of the scale band in Fig. 3(c)]. The competition between the capillary effect and the ES barrier effect gives rise to a dominant scale, which constitutes the dominant surface feature. To quantify the above observations, one needs to compute the scalegram (which is defined in Sec. II A). Figure 4 displays the scalegram evolution using the same integration parameters as above (Fig. 3). The figure clearly shows the existence of a dominant scale. In our example, the dominant scale is $l_d=3.5$. The final surface profile corresponds to the wavelet component at l_d, and it is represented at the inset of Fig. 4. In fact, the height profile derived from the solution of Eq. (15) is very much similar to the wavelet component at the scale l_d.

It is very important to stress that the ratio K/ν plays an important role in the growth process. If $K/\nu \gg 1$, the capillary effect dominates and the roughening mechanism becomes the noise-induced dynamic roughening (Mullins diffusion). For small K/ν, the ES barrier effect dominates. In fact, as shown in Fig. 5, as the ratio K/ν increases, the maximum of scalegram curves is hard to distinguish. This is an indication that the diffusion mechanism is dominating. Figure 6 shows the plot of the time evolution of the scalegram for some K/ν ratios. For large K/ν ratios, the dominant scale is hardly distinguished from the early stage of growth. However, for $K/\nu=1$, at the early stage of growth, the maximum is still not visible, but later on, a clear maximum is appearing. For small K/ν ratios (in which the ES barrier effect is dominating), the dominant scale is clearly visible from the early stages of growth. It is very interesting to note, from the plots in Fig. 6, the appearance of a critical scale as the ratio K/ν increases. Above this critical scale, the scalegram increases, meaning that large scale features are growing, while small scale features are decaying. The critical scale corresponds to the point in the scalegram graph where the branches split. For $K/\nu=5$ [Fig. 6(c)], the critical scale is $l_c \sim 5$.

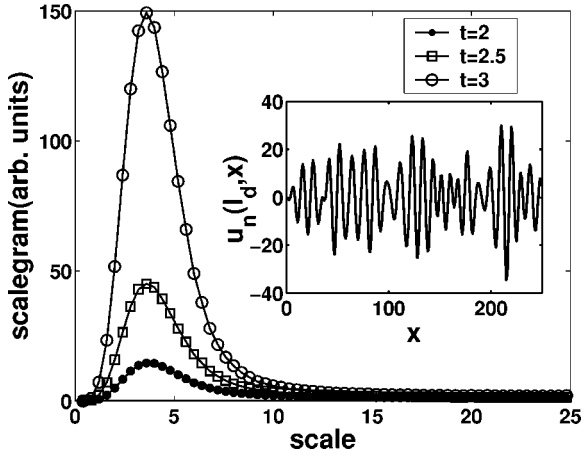

FIG. 4. The scalegram evolution of the growing front described by Eq. (2). The integration parameters are $\nu=1$, $D=0.05$, and $K=0.2$. The wavelet $g_2(x)$ is used in this calculation. The inset shows the wavelet component corresponding to the dominant scale.

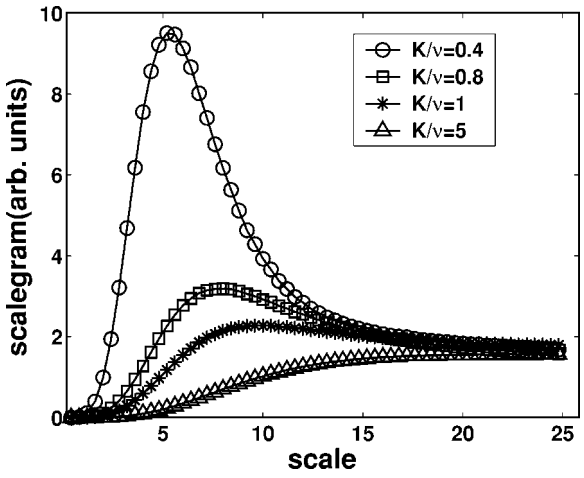

FIG. 5. The scalegram for different K/ν ratios for $t=3$. The wavelet $g_2(x)$ is used in this calculation.

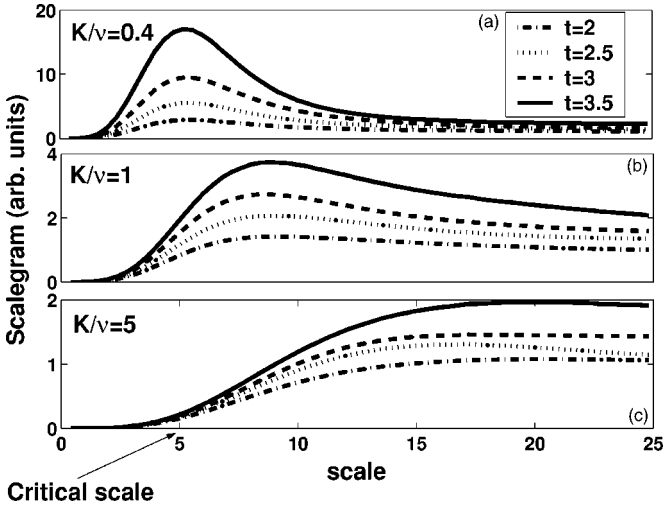

FIG. 6. Time evolution of the scalegram for $K/\nu=0.4$, 1, and 5 ratios. The wavelet $g_2(x)$ is used.

IV. EXPERIMENTAL EXAMPLE: ANISOTROPIC ETCHING OF SILICON

Although in the previous section our discussion was only focused on growth, we will discuss in this section the application of the above results to the chemical etching of silicon, which can be described by the anisotropic version of Eq. (2) [13] (the second-order term has two coefficients ν_x and ν_y, corresponding to the x and y direction, respectively). In this case, the parameter ν is related to the surface tension (the surface free energy density), while the parameter K is related to the energy of the formation of corners on the surface. We use the data for (110)-oriented silicon chemically etched with potassium hydroxide (KOH). A columnar structure on the surface is observed (as opposed to the mounds formation in the growth case). The height data are derived from atomic force microscope (AFM) images corresponding to different etching times. We calculate the scalegram in the x direction (perpendicular to the ripples orientation) for four different times: 40, 45, 50, and 55 min. The result is displayed in Fig. 7, where we clearly notice the existence of a critical scale l_c above which the scalegram increases, meaning that large-scale features are growing, while small-scale features are decaying. The critical scale corresponds to the point in the scalegram graph where the branches split, and it has the value $l_c=5$ μm. The scalegram clearly reveals that the etching of silicon(110) with KOH is unstable. It is noticed in Fig. 7 that the scalegram maximum, corresponding to the dominant scale, is not visible. This suggests that at this stage of etching, the effect of the corner interaction on the surface might be the dominating etching process. More experiments are needed to be carried out at longer etching times, especially when the effect of nonlinearity introduced by the lateral etching [the Kardar-Parisi-Zhang (KPZ) term] starts to be significant. This will be the subject of future investigations.

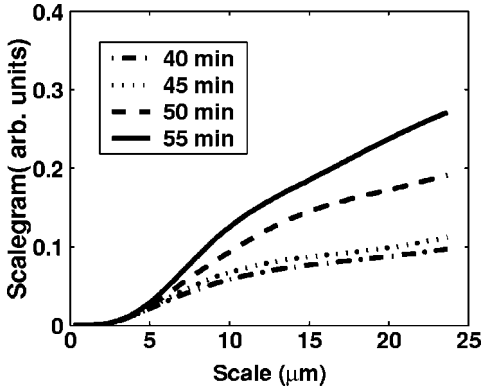

FIG. 7. The scalegram of chemically etched silicon showing the critical scale above which all surface features grow.

V. CONCLUSION

We have presented results concerning the characterization of unstable growing fronts using wavelet formalism. We have investigated the linear growth equation alongside an experimental example of the anisotropic etching of silicon. The unstable linear growth equation is transformed in wavelet space and the corresponding scalegram is computed. The scalegram is useful for the determination of the dominant and the critical scales of the growth process. Experimentally, the instability in silicon etching with KOH is revealed. We have determined the critical scale in this case, and find its value to be $l_c=5$ μm. Wavelet formalism has an advantage over Fourier methods in a way that one can track the instability in the location (direct space) and at different scales at the same time. It also provides a quantitative tool for the characterization of the growing fronts.

[1] Pimpinelli and J.Villain, *Physics of Crystal Growth* (Cambridge University Press, Cambridge, 1998).
[2] A. L. Barabasi and H. E. Stanly, *Fractal Concept in Surface Growth* (Cambridge University Press, Cambridge, 1995).
[3] P. Meakin, *Fractals, Scaling and Growth Far From Equilibrium* (Cambridge University Press, Cambridge, 1998).
[4] J. Villain, J. Phys. I **1**, 19 (1991).
[5] M. Kalff, P. Smilauer, G. Comsa, and T. Michely, Surf. Sci. **426**, L447 (1999).
[6] H. Jeong, S. Park, B. Kahng, and A.-L. Barabsi, Phys. Rev. Lett. **83**, 3486 (1999).
[7] R. Bradley and J. Harper, J. Vac. Sci. Technol. A **6**, 2390 (1988).
[8] J. Krug, Adv. Phys. **46**, 139 (1997).
[9] M. Makeev, R. Cuerno, and A.-L. Barabsi, Nucl. Instrum. Methods Phys. Res. B **197**, 185 (2002).
[10] P. Politi, G. Grenet, A. Marty, A. Ponchet, and J. Villain, Phys. Rep. **324**, 271 (2000).
[11] M. Elwenspoek and H. V. Jansen, *Silicon Micromachining* (Cambridge University Press, Cambridge, 1999).
[12] K. Sato, M. Shikida, T. Yamashiro, M. Tsunekawa, and S. Ito, Sens. Actuators, A **73**, 131 (1999).

[13] Z. Moktadir and K. Sato, Phys. Rev. B **64**, 033309 (2001).
[14] M. D. Johnson, C. Orme, A. W. Hunt, D. Graff, J. Sudijono, L. M. Sander, and B. G. Orr, Phys. Rev. Lett. **72**, 116 (1994).
[15] I. Daubechis, *Ten Lectures on Wavelets*, CBMS, NSF Series in Applied Mathematics (SIAM, Philadelphia, 2000).
[16] J. Lawalle, Phys. Rev. E **55**, 1590 (1997).
[17] J. Lawalle, Acta Mech. **104**, 1 (1994).